metals

MDPI

Article

Shape Memory Effect and Martensitic Transformation in Fe–Mn–Al–Ni Alloy

Rui Zhang, Deshan Sun, Chunmeng Ji, Yulin Chen, Xin Zhang * and Zhizhong Dong *

School of Materials Science and Engineering, Tianjin University of Technology, Tianjin 300384, China; zhangrui12312@126.com (R.Z.); deshan_sun@126.com (D.S.); 18920029096@163.com (C.J.); chenyulin@email.tjut.edu.cn (Y.C.)

* Correspondence: zhangxin3510110@tjut.edu.cn (X.Z.); zhizhong.dong@email.tjut.edu.cn (Z.D.); Tel.: +86-186-3087-8641 (X.Z.); +86-138-2037-1235 (Z.D.)

Abstract: In this study, the influence of an aging treatment on the shape memory effect and martensitic transformation was investigated in an Fe–Mn–Al–Ni alloy by adding a small amount of Nb and C elements. Results show that the aging treatment can significantly improve the shape recovery rate of the alloy. In the bending test with 4% deformation, after aging at 200 °C for 1 h, the recovery rate increased from 20 to 45%, and it further increased to 51% after the two-step aging treatment at 800 and 200 °C. The high-temperature in situ X-ray diffraction and atomic force microscope were used to reveal the shape memory effect between room temperature and 400 °C in this alloy due to $\gamma' \rightarrow \alpha$ transformation. The microstructure of aged specimens was investigated using transmission electron microscopy. With the extension of the aging time from 0.5 to 6 h, the size of NiAl precipitation gradually grew from 9 to 32 nm, and the distribution became more uniform. Meanwhile, the NbC particles were found in the two-step aging treatment alloy, which was the key to improving the shape memory effect.

Keywords: Fe–Mn–Al–Ni; martensitic transformation; shape memory effect; aging treatment

check for updates

Citation: Zhang, R.; Sun, D.; Ji, C.; Chen, Y.; Zhang, X.; Dong, Z. Shape Memory Effect and Martensitic Transformation in Fe–Mn–Al–Ni Alloy. *Metals* **2022**, *12*, 247. https://doi.org/10.3390/met12020247

Academic Editor: Shijie Hao

Received: 28 December 2021
Accepted: 25 January 2022
Published: 27 January 2022

Publisher's Note: MDPI stays neutral with regard to jurisdictional claims in published maps and institutional affiliations.

Copyright: © 2022 by the authors. Licensee MDPI, Basel, Switzerland. This article is an open access article distributed under the terms and conditions of the Creative Commons Attribution (CC BY) license (https://creativecommons.org/licenses/by/4.0/).

1. Introduction

Since Wayman first discovered the shape memory effect (SME) in FePt alloys [1], Fe-based shape memory alloys (SMAs) have been studied for more than 50 years. Studies dedicated to the SME of Fe-based SMAs have emerged in large numbers in recent years, such as FePd-, FeNiC-, FeNiCoTi- and FeMnSi-based alloys [2–6]. The cheap FeMnSi-based SMAs especially are expected to be the best potential alternative to NiTi-based SMAs and have been used for pipe couplings and fishplates [7]. However, the SME of FeMnSi-based SMAs is related to the fcc–hcp transition, exhibiting a non-thermoelastic martensitic transformation; thus, the alloys do not have superelasticity, which limits its engineering applications.

In 2011, Ando et al. doped a Ni element to Fe–Mn–Al alloys [8], and the NiAl phase was precipitated by an aging treatment, which was coherent with the matrix. In addition, NiAl precipitates strengthen the austenite matrix, hinder the dislocation during martensitic transformation, suppress the plastic deformation and induce the transformation to thermoelastic martensitic transformation, thus obtaining good superelasticity in Fe–Mn–Al–Ni alloys. Therefore, the critical stress of stress-induced martensitic transformation of Fe–Mn–Al–Ni alloys showed partial temperature dependence, which was only 0.5 MPa/°C. Because of this feature, this alloy exhibited good superelasticity over a wide temperature between −196 and 240 °C, and therefore expanded the application field [9,10].

In 2016, Omori found that the grain size increased significantly after cyclic heat treatment between a single-phase region (α phase) and a dual-phase region (α + γ phase). The cyclic heat treatment induced abnormal grain growth (AGG), achieving a bamboo-like structure in the alloy, which improved its superelasticity [11]. In 2019, Vollmer et al. doped

a 1.5 at.% Ti element to Fe–Mn–Al–Ni alloys. According to their research, the solid solution temperature of the γ phase decreased significantly, and the size of the subgrains became smaller, thereby obtaining a higher driving force for abnormal grain growth [12]. Recently, scientists have been focusing on improving superelasticity by adjusting heat treatment process and optimizing alloy composition [13–16]. Meanwhile, the potential applicability of the alloy has been investigated [17–20]. However, research on the shape memory effect has rarely been reported [21,22]. Therefore, further improvement of the shape memory effect is extremely necessary for the Fe–Mn–Al–Ni system.

In order to further improve the strength of the matrix and suppress the plastic deformation caused by the dislocation slip during the deformation process, in this study, we added a small amount of Nb and C elements to the Fe–Mn–Al–Ni alloy. After aging treatment, NbC particles were precipitated into the matrix; these second-phase particles could serve as nucleation points for stress-induced martensite, increasing the amount of martensite in the matrix, thereby promoting the occurrence of reverse phase transformation and improving the shape memory effect [23].

This investigation was dedicated to studying the effect of different aging treatments on the SME in the Fe–Mn–Al–Ni alloy. We observed the microstructure after tensile deformation and the evolution of martensitic plates during heating. In addition, we discussed the relationship between the SME and martensitic transformation and studied the effect of the precipitations on the property.

2. Materials and Methods

The specimen used in this research was the as-cast Fe–Mn–Al–Ni alloy. The composition is shown in Table 1. The ingot was prepared by vacuum induction melting, and then it was homogenized in a vacuum furnace at 1100 °C for 10 h. Next, a specimen of appropriate size was cut from the alloy and sealed in a quartz tube filled with argon, and then the solution was treated at 1200 °C for 2 h, followed by water cooling. The bending test specimen with a size of 45 × 3 × 0.7 mm and a dog-bone-shaped tensile specimen with a size of 1 × 3.5 × 50 mm were cut by a wire electric discharge machine. These specimens aged at 200 °C and 800 °C + 200 °C, respectively. The dog-bone-shaped specimen was subjected to tensile test by a GNT50 testing machine (NCS, Beijing, China) with a pre-strain of 4%, and the critical stress of stress-induced martensitic transformation was calculated by the 0.2% strain offset method. The shape memory effect was examined by a bending test with a deformation of 4%. Firstly, these specimens after aging treatment were deformed at room temperature and measured for the elastic recovery angle (θ_e) after unloading; secondly, specimens were heated between 100 and 400 °C, for which the holding time was 10 min; finally, the shape recovery angle (θ_r) was measured after air cooling to room temperature.

Table 1. Chemical composition of Fe–Mn–Al–Ni alloy (at.%).

Fe	Mn	Al	Ni	Nb	C
41.03	35.4	14.8	7.9	0.8	0.07

The phases were determined by D8 ADVANCE high-temperature in situ X-ray diffraction (XRD) (Bruker, Karlsruhe, Germany). The $\gamma' \rightarrow \alpha$ transformation was observed with the Dimension Icon atomic force microscope (AFM). (Bruker, Karlsruhe, Germany). A JEM-2100 transmission electron microscope (TEM) (JEOL, Tokyo, Japan) was employed to observe the microstructures of the aged specimens.

3. Results and Discussion

3.1. Shape Memory Effect

Figure 1a shows the shape recovery rate of the alloy under different aging treatment conditions. It can be seen from Figure 1 that the recovery rate showed a rising trend with the increase in heating temperature. When the heating temperature rose to 400 °C, the recovery

rate of the alloy reached its maximum. Further, we observed that the aging treatment can significantly improve the recovery rate, and the maximum recovery rate was about 45% when the alloy aged at 200 °C for 1 h.

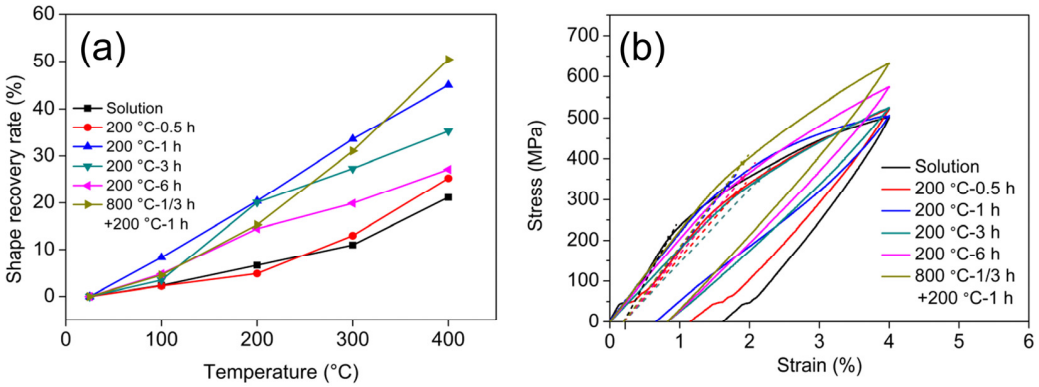


Figure 1. Shape recovery rate and stress–strain curves of tensile test of alloys with different aging conditions. (**a**) Shape recovery rate of the alloy. (**b**) Stress–strain curves of alloy after 4% pre-strain tension.

In order to investigate the effect of NbC particles on the SME, the alloy aged at 800 °C for 20 min first and then aged at 200 °C for 1 h. As shown in Figure 1a, it can be concluded that the recovery rate also showed a rising trend with the increase in heating temperature. Moreover, the recovery rate of the alloy after aging at 800 °C for 20 min increased slightly, and when the heating temperature was 400 °C, the shape recovery rate increased from 45 to 51%.

Figure 1b shows the stress–strain curves of the alloy after 4% pre-strain tension. It was calculated by the 0.2% strain offset method that the critical stress for stress-induced martensitic transformation of the solution specimen was 206 MPa, and after the aging treatment, the critical stress increased significantly, reaching 353 MPa after aging at 200 °C for 6 h. Moreover, the critical stress further increased to 389 MPa after the specimen received the two-step aging treatment.

3.2. $\gamma' \rightarrow \alpha$ Transformation Behavior

In order to study the evolution of microstructure during heating, the specimens, which were heated at different temperatures, were subjected to phase analysis by high-temperature in situ XRD. As shown in Figure 2, with the increase in temperature, the intensity of the (111)γ' peak decreased gradually. In addition, the (110)α peak with lower intensity occurred when the specimens were heated at 300 °C. It was found by calculation that when the temperature increased from 300 to 400 °C, the percentage of the γ' phase decreased from 82.6 to 76.1, and the percentage of the α phase increased from 17.4 to 23.9. Accordingly, this indicates that the amount of stress-induced γ' martensite reduced gradually and the $\gamma' \rightarrow \alpha$ transformation occurred.

In order to further investigate the reason for the occurrence of the SME, we conducted a room-temperature tensile experiment. In addition, atomic force microscopy was used to observe martensite relief on the surface of the specimen after 4% pre-strain was applied. Figure 3a shows the AFM picture of a specimen after experiencing 4% pre-strain; it can be seen that several parallel martensitic plates appeared on the surface of tensile specimens. Figure 3b shows the cross-section curve along the line in Figure 3a, from which the tilt angles for plates A, B, C, D and E in Figure 3a were measured to be 3.5°, 5.1°, 3.4°, 4.1° and 3.8°, respectively. Therefore, we can infer that these martensitic plates belong to the same type of martensitic variant. Figure 3c–f show the martensitic reverse transformation. It was found that the amount of γ' martensite gradually reduced, and the width of the martensitic plates decreased with the increase in temperature. When the heating temperature reached 400 °C, the martensitic plates almost disappeared completely. This indicates that γ' martensitic

transforms back to the α phase during heating. This is consistent with the results observed by XRD. This can explain the results observed in the bending experiment. When the temperature rose, the reverse transformation of $\gamma' \rightarrow \alpha$ occurred, which shows the specimen returned to its initial shape.

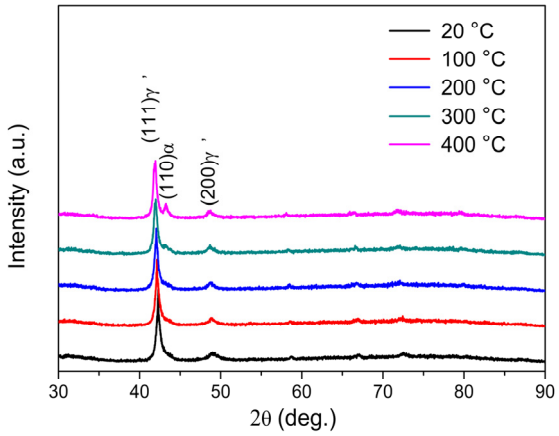


Figure 2. High-temperature in situ XRD pattern of the tensile specimens at different temperatures.

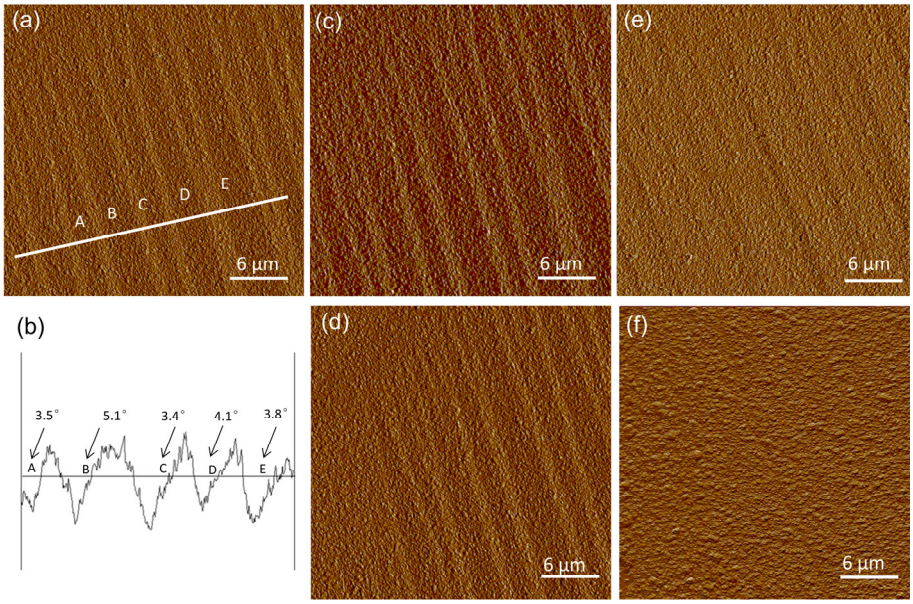


Figure 3. AFM micrographs of specimens with 4% pre-strain tension at different temperatures and martensitic relief angles. (**a**) Room temperature. (**b**) Cross-section curve of the surface along white line in (**a**,**c**,**d**–**f**). The same site in (**a**) after heating to 100 °C, 200 °C, 300 °C and 400 °C, respectively.

3.3. Investigation of Precipitation

As mentioned above, the shape recovery rate and the critical stress of the stress-induced martensitic transformation of the alloy after the aging treatment have been improved. In order to determine the reason behind the performance improvement, TEM as employed to investigate the microstructures. Figure 4 depicts the TEM bright-field image of precipitations under different aging treatment conditions and the corresponding selected area diffraction (SAED) pattern of the alloy aged at 200 °C for 6 h. It was found from the pattern that there were diffraction spots in the austenite matrix, and there was a weak NiAl precipitation spot in the center of the matrix spot.

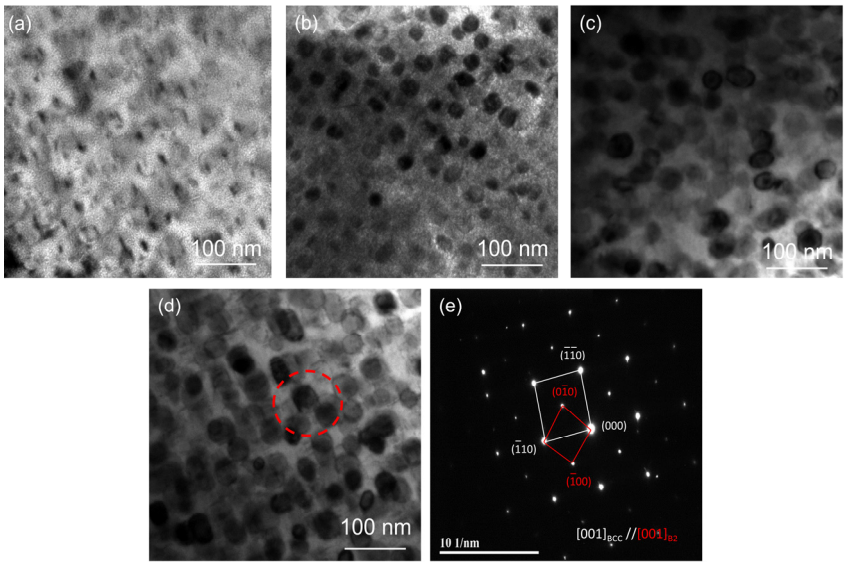


Figure 4. Morphology of precipitations and SAED patterns of the alloy under different aging conditions: (**a**) 200 °C-0.5 h, (**b**) 200 °C-1 h, (**c**) 200 °C-3 h and (**d**) 200 °C-6 h. (**e**) The corresponding SAED of precipitations in (**d**).

It can be seen from Figure 4a that when the aging conditions were 200 °C for 0.5 h, the precipitations with a size of about 8 nm were precipitated from the matrix. After aging at 200 °C for 1 h and 3 h, the size of precipitations increased to 23 and 28 nm, respectively (Figure 4b,c). With the continuous increase in the aging time, the precipitations gradually grew and were distributed more uniformly. The size of the precipitations increased to about 32 nm when the aging time was 6 h (Figure 4d).

According to the above SME experimental results, as shown in Figure 1a, a trend of first rising and then falling can be seen with the extension of the aging treatment time when the specimens aged at 200 °C. This phenomenon is related to the size of the precipitations; when the aging time was short, the size of the precipitations was only 8 nm (Figure 4a), but these fine precipitations could strengthen the matrix and suppress plastic deformation to some extent, so the shape recovery rate increased slightly compared to the solution-treated specimens. With the increase in aging time, the size of NiAl precipitations became larger, reaching about 25 nm (Figure 4b,c), and the distribution became more uniform, which further strengthened the matrix and suppressed the plastic deformation, thus promoting the shape recovery rate. However, with the further extension of aging time, the precipitation grew and coarsened continuously, reaching a size of about 32 nm (Figure 4d); the strengthening effect decreased because the coherent relationship with the matrix was destroyed, and the large-size precipitations reduced the resistance to dislocation movement, so the shape recovery rate decreased. However, as the number of NiAl precipitations gradually increased, these fine and uniformly distributed precipitations significantly increased the strength of the austenite matrix, thereby increasing the critical stress of the stress-induced martensitic transformation of the alloy (Figure 1b).

As shown in Figure 1a, the shape recovery rate of the alloy increased from 45 to 51% after the two-step aging treatment. Therefore, TEM observation was performed on the alloy that underwent the two-step aging treatment as shown in Figure 5a. Figure 5b,c portray the SAED spots of areas 1 and 2 in Figure 5a, respectively. It can be seen that the dark NbC particles were precipitated after aging at 800 °C. Through the SAED, it can be inferred that NbC and NiAl precipitations, which precipitated in the matrix after two-step aging, and some NbC precipitations are associated with the NiAl phase. In addition, long strips of the NiAl phase were also found in the alloy that experienced the two-step aging treatment.

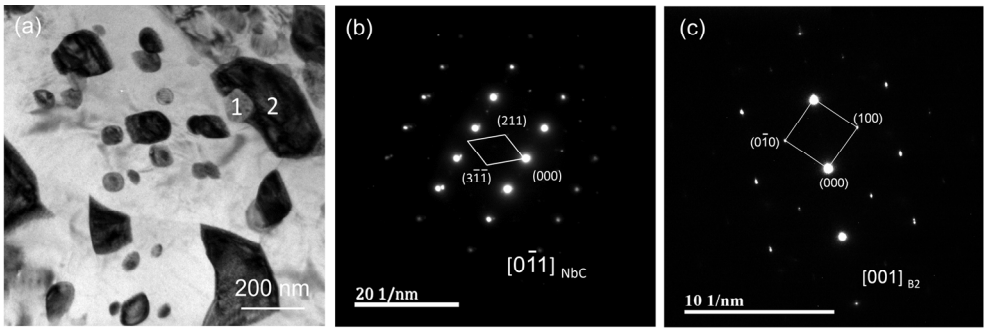


Figure 5. Morphology and SAED patterns of precipitations after two-step aging treatment. (**a**) Morphology of precipitations (**b**) and (**c**) the SAED of area 1 and 2 in (**a**), respectively.

We found NbC and NiAl particles in the matrix after the alloy received the two-step aging treatment. These two kinds of precipitations can not only strengthen the matrix but also suppress the generation of slip during the deformation process. Secondly, the NbC particles may be the nucleation site of the stress-induced martensitic transformation and may reduce the stress-induced martensitic transformation critical stress. Besides, it is likely that the same type of martensitic variant is activated at each grain throughout the austenite. At the same time, the elastic stress field forms around the particles, which will generate a driving force at the tip of the martensite to promote the recovery of dislocations. It can restrain the excessive growth of martensite, which is conducive to the occurrence of reverse martensitic transformation and improves the shape recovery rate [24–27]. Since NbC and NiAl particles together can strengthen the matrix, the critical stress of stress-induced martensitic transformation of the alloy further increased after the two-step aging treatment.

4. Conclusions

In this study, the influence of an aging treatment on the shape memory effect and martensitic transformation was investigated in an Fe–Mn–Al–Ni alloy with a small amount of Nb and C elements. The following conclusions were drawn:

(1) Through the SME test, we found that aging treatment can significantly improve recovery rate; when the specimens aged at 200 °C for 1 h, the maximum recovery rate increased from 20 to 45% In addition, when the two-step aging treatment was carried out at 800 and 200 °C, the recovery rate further increased to 51%.

(2) AFM results show the surface relief of martensitic plates and measurements of the single-variant martensitic plates are produced by tension. The AFM and high-temperature in situ XRD analyzed the amount of stress-induced γ' martensite reduced during heating and exhibited the SME resulting from the transformation of $\gamma' \rightarrow \alpha$.

(3) TEM results show that the NiAl phase was precipitated in the matrix when the alloy aged at 200 °C; with the extension of the aging treatment time from 0.5 to 6 h, the size of the precipitations grew from 9 to 32 nm. In addition, NbC particles were found in the two-step aging treatment alloy. These particles can strengthen the matrix and serve as the nucleation point of the martensitic transformation. Simultaneously, the elastic stress field generated around the NbC precipitations was conducive to the occurrence of the reverse martensitic transformation.

Author Contributions: Conceptualization, D.S. and R.Z.; Methodology, C.J. and Y.C.; Investigation, D.S.; Data curation, R.Z.; Formal analysis, R.Z. and Z.D.; Writing—original draft Preparation, R.Z.; Writing—Review and Editing, X.Z. and Z.D.; Funding acquisition, X.Z.; Supervision, Z.D. All authors have read and agreed to the published version of the manuscript.

Funding: This research was funded by the National Natural Science Foundation of China (Grant No. 52071236).

Institutional Review Board Statement: Not applicable.

Informed Consent Statement: Not applicable.

Data Availability Statement: Data sharing not applicable. No new data were created or analyzed in this study. Data sharing is not applicable to this article.

Acknowledgments: The authors acknowledge the financial support from by the National Natural Science Foundation of China (Grant No. 52071236).

Conflicts of Interest: The authors declare no conflict of interest.

References

1. Dunne, D.P.; Wayman, C.M. The effect of austenite ordering on the martensite transformation in Fe-Pt alloys near the composition Fe_3Pt: I. Morphology and transformation characteristics. *Metall. Trans.* **1973**, *4*, 137–145. [CrossRef]
2. Guler, E.; Kirindi, T.; Aktas, H. Comparison of thermally induced and deformation induced martensite in Fe-29% Ni-2% Mn alloy. *J. Alloy. Compd.* **2007**, *440*, 168–172. [CrossRef]
3. Oliver, E.C.; Mori, T.; Daymond, M.R.; Withers, P.J. Neutron diffraction study of stress-induced martensitic transformation and variant change in Fe-Pd. *Acta Mater.* **2003**, *51*, 6453–6464. [CrossRef]
4. Maki, T.; Kobayashi, K.; Minato, M.; Tamura, I. Thermoelastic martensite in an ausaged Fe-Ni-Ti-Co alloy. *Scr. Mater.* **1984**, *18*, 1105–1109. [CrossRef]
5. Abuzaid, W.; Sehitoglu, H. Superelasticity and functional fatigue of single crystalline FeNiCoAlTi iron-based shape memory alloy. *Mater. Des.* **2018**, *160*, 642–651. [CrossRef]
6. Baruj, A.; Kikuchi, T.; Kajiwara, S.; Shinya, N. Improvement of shape memory properties of NbC containing Fe-Mn-Si based shape memory alloys by simple thermomechanical treatments. *Mater. Sci. Eng. A* **2004**, *378*, 333–336. [CrossRef]
7. Maruyama, T.; Kurita, T.; Kozaki, S.; Andou, K.; Farjami, S.; Kubo, H. Innovation in producing crane rail fishplate using Fe-Mn-Si-Cr based shape memory alloy. *Mater. Sci. Technol.* **2008**, *24*, 908–912. [CrossRef]
8. Omori, T.; Ando, K.; Okano, M.; Xu, X.; Tanaka, Y.; Ohnuma, I.; Kainuma, R.; Ishida, K. Superelastic Effect in Polycrystalline Ferrous Alloys. *Science* **2011**, *333*, 68–71. [CrossRef]
9. Omori, T.; Nagasako, M.; Okano, M.; Endo, K.; Kainuma, R. Microstructure and martensitic transformation in the Fe-Mn-Al-Ni shape memory alloy with B2-type coherent fine particles. *Appl. Phys. Lett.* **2012**, *101*, 231907. [CrossRef]
10. Ando, K.; Omori, T.; Ohnuma, I.; Kainuma, R.; Ishida, K. Ferromagnetic to weak-magnetic transition accompanied by bcc to fcc transformation in Fe-Mn-Al alloy. *Appl. Phys. Lett.* **2009**, *95*, 212504. [CrossRef]
11. Omori, T.; Iwaizako, H.; Kainuma, R. Abnormal grain growth induced by cyclic heat treatment in Fe-Mn-Al-Ni superelastic alloy. *Mater. Des.* **2016**, *101*, 263–269. [CrossRef]
12. Vollmer, M.; Krooß, P.; Karaman, I.; Niendorf, T. On the effect of titanium on quenching sensitivity and pseudoelastic response in Fe-Mn-Al-Ni-base shape memory alloy. *Scr. Mater.* **2017**, *126*, 20–23. [CrossRef]
13. Tseng, L.W.; Ma, J.; Vollmer, M.; Krooß, P.; Niendorf, T.; Karaman, I. Effect of grain size on the superelastic response of a FeMnAlNi polycrystalline shape memory alloy. *Scr. Mater.* **2016**, *125*, 68–72. [CrossRef]
14. Ozcan, H.; Ma, J.; Karaman, I.; Chumlyakov, Y.I.; Santamarta, R.; Brown, J.; Noebe, R.D. Microstructural design considerations in Fe-Mn-Al-Ni shape memory alloy wires: Effects of natural aging. *Scr. Mater.* **2018**, *142*, 153–157. [CrossRef]
15. Ozcan, H.; Ma, J.; Wang, S.J.; Karaman, I.; Chumlyakov, Y.; Brown, J.; Noebe, R.D. Effects of cyclic heat treatment and aging on superelasticity in oligocrystalline Fe-Mn-Al-Ni shape memory alloy wires. *Scr. Mater.* **2017**, *134*, 66–70. [CrossRef]
16. Xia, J.; Noguchi, Y.; Xu, X.; Odaira, T.; Kimura, Y.; Nagasako, M.; Omori, T.; Kainuma, R. Iron-based superelastic alloys with near-constant critical stress temperature dependence. *Science* **2020**, *369*, 855–858. [CrossRef] [PubMed]
17. Vollmer, M.; Bauer, A.; Frenck, J.M.; Krooß, P.; Wetzel, A.; Middendorf, B.; Fehling, E.; Niendorf, T. Novel prestressing applications in civil engineering structures enabled by Fe-Mn-Al-Ni shape memory alloys. *Eng. Struct.* **2021**, *241*, 112430. [CrossRef]
18. Vollmer, M.; Bauer, A.; Kriegel, M.J.; Motylenko, M.; Niendorf, T. Functionally graded structures realized based on Fe-Mn-Al-Ni shape memory alloys. *Scr. Mater.* **2021**, *194*, 113619. [CrossRef]
19. Mandel, M.; Kietov, V.; Hornig, R.; Vollmer, M.; Frenck, J.M.; Wustefeld, C.; Rafaja, D.; Niendorf, T.; Kruger, L. On the polarisation and Mott-Schottky characteristics of an Fe-Mn-Al-Ni shape-memory alloy and pure Fe in NaCl-free and NaCl-contaminated $Ca(OH)_{2,sat}$ solution-A comparative study. *Corros. Sci.* **2021**, *179*, 109172. [CrossRef]
20. Popa, M.; Mihalache, E.; Cojocaru, V.D.; Gurau, C.; Gurau, G.; Cimpoesu, N.; Pricop, B.; Comaneci, R.I.; Vollmer, M.; Krooß, P.; et al. Effects of thermomechanical processing on the microstructure and mechanical properties of Fe-based alloys. *J. Mater. Eng. Perform.* **2020**, *29*, 2274–2282. [CrossRef]
21. Huang, P.; Peng, H.B.; Wang, S.L.; Zhou, T.N.; Wen, Y.H. Relationship between martensitic reversibility and different nano-phases in a FeMnAlNi shape memory alloy. *Mater. Charact.* **2016**, *118*, 22–28. [CrossRef]
22. Peng, H.B.; Huang, P.; Zhou, T.N.; Wang, S.L.; Wen, Y.H. Reverse shape memory effect related to $\alpha \rightarrow \gamma$ transformation in a Fe-Mn-Al-Ni shape memory alloy. *Mater. Trans. A* **2017**, *48*, 2132–2139. [CrossRef]
23. Kajiwara, S.; Liu, D.; Kikuchi, T.; Shinya, N. Remarkable improvement of shape memory effect in Fe-Mn-Si based shape memory alloys by producing NbC precipitates. *Scr. Mater.* **2001**, *44*, 2809–2814. [CrossRef]

24. Baruj, A.; Kikuchi, T.; Kajiwara, S. TEM observation of the internal structures in NbC containing Fe–Mn–Si-based shape memory alloys subjected to pre-deformation above room temperature. *Mater. Sci. Eng. A* **2004**, *378*, 337–342. [CrossRef]
25. Stanford, N.; Dunne, D.P. Effect of NbC and TiC precipitation on shape memory in an iron-based alloy. *J. Mater. Sci.* **2006**, *41*, 4883–4891. [CrossRef]
26. Stanford, N.; Dunne, D.P. Effect of second-phase particles on shape memory in Fe-Mn-Si-based alloys. *Mater. Sci. Eng. A* **2007**, *454*, 407–415. [CrossRef]
27. Ogawa, K.; Sawaguchi, T.; Kikuchi, T.; Kajiwara, S. Mechanism of improvement of shape memory effect in NbC containing Fe-Mn-Si-based shape memory alloys. *J. Jpn. Inst. Met.* **2006**, *70*, 25–33. [CrossRef]